J Mater Sci (2010) 45:6604–6610
DOI 10.1007/s10853-010-4750-7

Study of internal stresses in a TWIP steel analyzing transient and permanent softening during reverse shear tests

I. Gutierrez-Urrutia · J. A. del Valle · S. Zaefferer · D. Raabe

Received: 28 April 2010 / Accepted: 5 July 2010 / Published online: 17 July 2010

Abstract Recent Bauschinger-type tests conducted on a twinning-induced plasticity (TWIP) steel highlights the important contribution of internal stresses to work hardening [1]. Along this line we present Bauschinger experiments in a Fe–22Mn wt%–0.6C wt% TWIP steel. The mechanical behavior upon load reversal shows transient and permanent softening effects. Determination of the internal stress from the magnitude of the permanent softening yields a contribution to work hardening of the order of 20%. Analysis of the transient softening, during strain reversal, indicates that internal stress is consistent with reported data on high carbon spheroidized steels.

Introduction

Twinning-induced plasticity (TWIP) steels obtain their outstanding mechanical properties from the enhancement of the work hardening rate due to the formation of bundles of mechanical nanotwins during straining [2–6]. Such dynamical microstructural refinement produces an increasing interaction between glide dislocations and twin boundaries acting as strong barriers. This mechanism is usually termed "dynamic Hall–Petch" (DHP) because twin boundaries contribute to hardening such as grain boundaries in a polycrystal do, and the twin spacing decreases during straining due to the increase of the twin fraction [7].

I. Gutierrez-Urrutia · S. Zaefferer · D. Raabe
Max-Planck-Institut für Eisenforschung, Max-Planck Str. 1, 40237 Düsseldorf, Germany

J. A. del Valle (✉)
CENIM-CISC, Avenida Gregorio del Amo 8, 28040 Madrid, Spain
e-mail: delvalle@cenim.csic.es

In addition to this isotropic hardening mechanism a recent report by Bouaziz et al. [1], based on Bauschinger-type shear test in a Fe–22Mn wt%–0.6C wt% TWIP steel, suggests that an important additional, viz kinematic hardening contribution should be taken into account [8].

The difference in forward and subsequent reverse flow stresses, referred to as Bauschinger effect (BE), is often attributed to the development of internal polarized stresses, named back stresses. These stresses oppose to flow stress in forward straining but aid in reverse straining. The development of this stress contribution is also termed kinematic hardening because it produces a translation of the yield surface under strain reversal [9]. The dependence of stress on strain path should be included in the analysis of the forming process, work hardening models and related phenomena [10–13].

A Von Mises equivalent back stress contribution of around 450 MPa at 0.2 equivalent strain, which corresponds to about half of the total flow stress, was reported for Fe–22Mn wt%–0.6C wt% TWIP steel with a grain size of 3 μm [1]. Taking into account the initial yield stress of 400 MPa, this implies that back stresses represent 3/4 of the total work hardening developed at this strain level, being the remaining 1/4 corresponding to the DPH and forest dislocation hardening. This high internal stress contribution was explained in terms of dislocations that accumulate before twin boundaries upon plastic loading [1] which then in turn give rise to the back stress as Orowan loops do in the well known case of materials containing impenetrable particles [14, 15]. However, Bouaziz et al. reported back stresses remarkably higher than values reported by Wilson and Bate [16], in the range 200–250 MPa, determined by X-ray diffraction in steels with a high volume fraction of cementite particles. In the present work, we provide new experimental results on the

contribution of back stresses to the flow stress in a Fe–22Mn wt%–0.6C wt% TWIP steel. The Bauschinger effect (BE) is evaluated by performing strain shear reversal tests at room temperature. The reverse curves reveal both the transient and permanent softening effects. Determination of the back stress from the magnitude of the permanent softening yields a contribution of the kinematic hardening to the total work hardening of around 20%. Additionally, an important effect of grain size, and probably texture, on permanent softening is shown. Comparison of the transient softening with data reported on spheroidized steels [16] shows that in the present TWIP steel no outstanding BE occurs.

Experimental details

The material used in this study was a Fe–22Mn–0.6C twinning induced plasticity (TWIP) steel (in wt%). The material was melted in an induction furnace under Ar atmosphere and cast to round bars of 25 mm in diameter. To avoid Mn segregation, [17] samples were swaged to 20% area reduction at 1000 °C and subsequently solution-treated for 4 h at 1100 °C under Ar. Thereafter, samples were hot-rolled to 75% reduction in thickness at 1000 °C followed by air cooling. The material had a recrystallized structure with an average grain size of 50 μm [6].

Figure 1a shows a scanning electron microscope micrograph using back-scattered electrons of the studied material and Fig. 1b shows the inverse pole figures of hot-rolled material obtained by electron back scatter diffraction (EBSD).

The simple shear test is an efficient method to evaluate the BE in metallic materials. In recent years, most reports on the analysis of BE have been performed using shear test instead of tension–compression test because shear test allows applying high strains in forward and subsequent reverse directions avoiding necking effects related to plastic instabilities. For this reason, in the present work the BE was studied by means of shear reversal testing. These tests were carried out in an in-house set-up inspired in previous works [18–20]. The device, presented in Fig. 2, is located directly in a Servosis screw-driven test machine. The movable grip displaces vertically (horizontal movement is not allowed) keeping the sample centered and deformed under pure shear strain. Samples fit precisely in the grip holder and additional clamping of the sample is obtained by the tightening of screws, as it is shown in the right side of Fig. 2b. Vertical displacement, ΔL, was measured by clamping an extensometer onto the grips (not shown in this figure). Samples have a rectangular shape of $L \times H \times E = 40 \times 14 \times 2$ mm^3 (for notation see Fig. 2c). In order to avoid any damage of the shear zone when gripping the samples, a calibrated shear zone of $L \times h \times e = 40 \times 3 \times 1$ mm^3 (for notation see Fig. 2c) was machined out by electrical discharge as it is depicted in Fig. 2c [18]. The shear stress–strain curve was obtained from the force–displacement curves using $\gamma = \Delta L/h$ and $\tau = F/\text{Le}$. A constant strain rate of $\dot{\gamma} = 5 \times 10^{-3}\text{s}^{-1}$ was imposed during tests.

Results and discussion

Analysis of the reverse shear tests data

Figure 3a shows the Wilson's plot [21] given by the representation of the monotonic forward shear stress–strain curve and the reflected reverse curves from reverse test, performed at different forward pre-strain levels. It can be seen that the curves becomes parallel after a reverse shear plastic strain γ_r. The offset between these two curves for $\gamma > \gamma_r$, given by $\tau - \tau_{rev}$, is referred to as "permanent softening" [15, 16, 21, 22]. The softening in the zone of

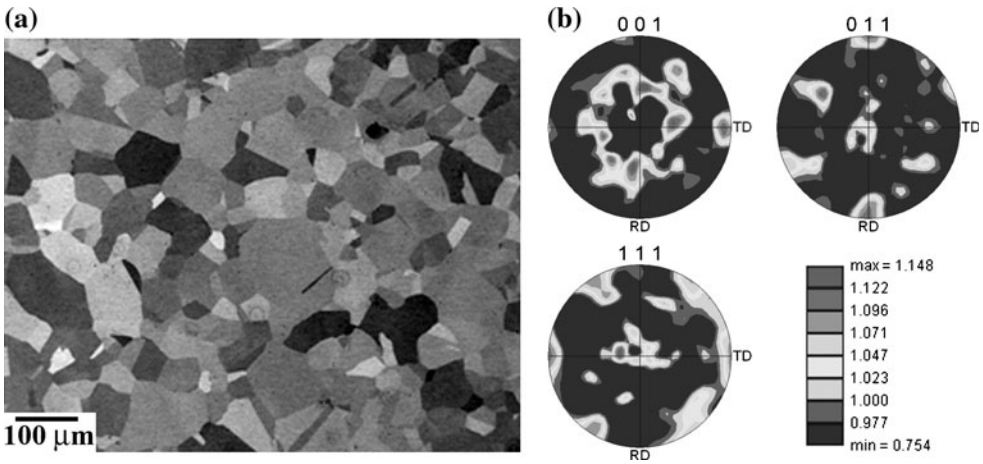

Fig. 1 **a** Scanning electron microscopy image using backscattered electrons of the microstructure of the hot-rolled material. **b** Inverse pole figures of as hot-rolled material determined by electron back scatter diffraction (EBSD). RD = rolling direction, TD = transverse direction

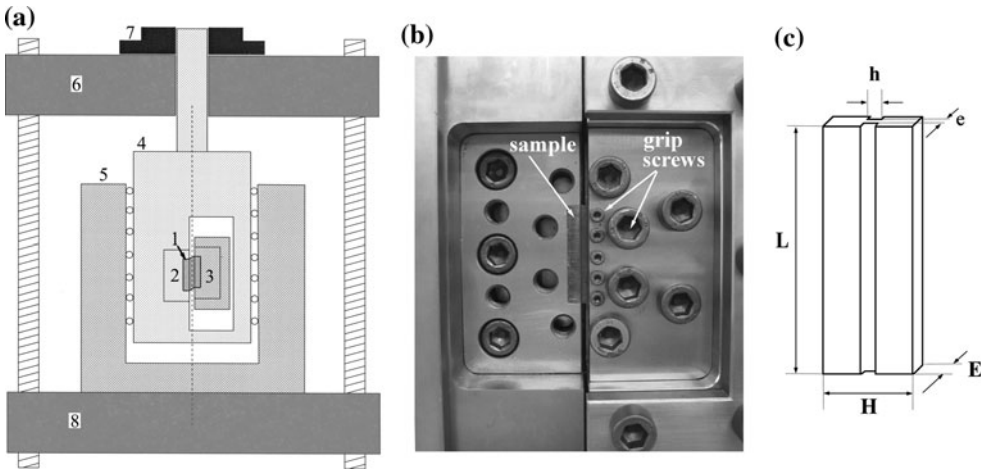

Fig. 2 **a** Schematic overview of the shear test device: *1* sample, *2* movable grip, *3* fixed grip, *4* upper movable frame part, *5* lower fixed frame part, *6* test machine crosshead, *7* load cell, *8* test machine floor. **b** Photograph of the shear device and the grip system. **c** Geometry of shear samples

$\gamma < \gamma_r$ is termed "transient softening". This graph clearly shows that in the present TWIP steel, the permanent softening effect occurs after a reverse plastic strain close to one-half the forward pre-strain.

Figure 3b shows equivalent stress–equivalent plastic strain curves, σ_{eq} versus ε_{eq}, of experimental data taken from Bouaziz's work [1] corresponding to exactly the same TWIP steel than the studied in this work but with a finer grain size of 3 μm. Von Mises equivalent stress–strain curves are derived from shear stress–shear strain, τ versus γ, curves using the relations [18]:

$$\sigma_{eq} \approx 3^{1/2}\tau \tag{1}$$

$$\varepsilon_{eq} = \gamma/\left(3^{1/2}\right) \tag{2}$$

Comparison of the experimental data shown in Fig. 3a with those presented in Fig. 3b shows that the permanent softening effect observed in the present work is much lower than that obtained from Bouaziz's data. However, in both data sets the permanent softening effect is clearly present.

The BE is generally analyzed as follows. The back stress, τ_b, in the matrix make an additive contribution to the flow stress during forward strain, which can be written as [1, 16, 22, 23]:

$$\tau = \tau_o + \tau_f + \tau_b \tag{3}$$

where τ_o is the initial yield stress including the matrix friction stress, solid solution hardening and Hall–Petch hardening. The stress τ_f is the forest hardening. Both hardening contributions, τ_o and τ_f, are considered to be isotropic, i.e., non-polarized. In the present case of a TWIP steel, Eq. 3 should include an additional isotropic contribution, arising from the DHP effect.

The hardening contribution, τ_b, is polarized, i.e., it favors deformation in reverse sense. When the sense of the deformation is reversed, after some strain, the plastic deformation can be considered to occur at the following stress:

$$\tau_{rev} = \tau_o + \tau_f - \tau_b \tag{4}$$

The back stress term is thus obtained from Eqs. 3 and 4:

$$\tau_b = (\tau - \tau_{rev})/2 \tag{5}$$

The BE has been previously reported in several particle-hardened materials [16, 21–31], and even in steels containing twins [1, 32]. Nevertheless, the rationalization of the BE results is not straightforward. The major concern is the determination of an adequate reverse strain in order to obtain τ_{rev} and τ_b. The pioneering work by Atkinson et al. [22] in Cu–SiO_2 demonstrates that the magnitude of

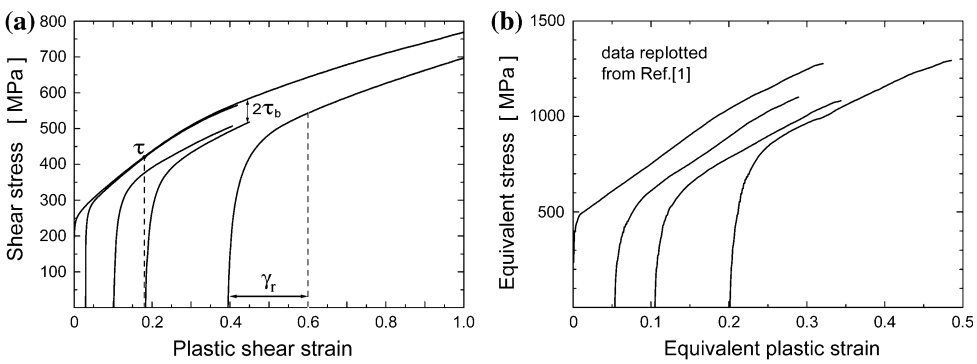

Fig. 3 **a** Bauschinger curves obtained from shear test. Reverse curves are plotted with the flow stress positive to show the permanent softening effect. **b** Data extracted from Ref. [1] and replotted to show the permanent softening effect

the back stress, obtained by measurements of the permanent softening and applying Eq. 5, coincides with the results of internal stresses obtained from X-ray determinations by Wilson [21]. However, further experimental evidence based on X-ray measurements [16] put into question the relationship between the permanent softening and back stress. Additionally, in some materials, the forward and reverse curves never become truly parallel [23, 26]. In that case, the analysis was carried out assuming a given reverse offset strain in order to obtain σ_{rev} and, successively, σ_b [23, 32]. The analytical difficulties associated with the interpretation of the BE were revisited by Pragnell et al. [27]. The relationship between the permanent softening and the back stress holds when the matrix work hardening rate is unaffected by changes in the sense of plastic strain, and when back stresses are eliminated upon load reversal at the same rate as generated during forward loading [27]. Therefore, there is no incontrovertible definition of the reverse strain at which the $\tau - \tau_{rev}$ can be related to back stresses, making the derivation of the internal stresses from the BE a challenging task in these materials.

However, when the reverse curve becomes parallel to the forward curve at low reverse strains, typically in the range 0.3-0.5 times the forward strain, there is good agreement between the back stress estimated from the permanent softening measurements and that calculated from X-ray diffraction data [16, 22]. Otherwise, when the parallel course between the reverse and forward curve occurs at large reversal strains (around 2–5 times the forward strain), a remarkable high difference is observed between the back stress values calculated from the permanent softening measurements and those calculated from X-ray diffraction data (as high as 2 times) [16].

Figure 4 shows the evolution of the transient softening during reverse strain for the present TWIP steel and the Bouaziz's et al. steel. As it can be seen, both steels exhibit similar values of transient softening for very small values of $\varepsilon_{rev}/\varepsilon_o < 0.05$. However, with increasing reverse strain, these materials develop very different values of permanent softening.

Figure 5 summarizes the evolution of the equivalent back stress with the equivalent deformation calculated from relations (5) and (1). These data were determined using two different approaches: calculations from permanent softening measurements and from the strain–stress curves by the use of an offset reverse strain of 0.2%. It must be pointed out that Bouzaiz et al. [1] did not specify the offset strain. However, from the analysis of the data digitalized from Ref. [1] it can be deduced that an offset strain of 0.2% was used in that work. This figure reveals that the values of back-stresses determined by means of the 0.2% offset strain approach are similar in both materials. These values are up to 3 times higher than those obtained from permanent softening determinations. This difference is usual in reverse straining tests, due to yielding occurrence at the early portion of the reverse strain curve [23, 27]. Thus, as discussed above, the determination of back stresses from the BE is very sensitive to the reverse strain at which back stress is measured [23].

Restricting the analysis to the data obtained by permanent softening measurements, an important result is found: back stresses obtained in the present work are approximately half those in the Bouaziz's TWIP steel. In the present case, parallel course of the forward and reverse flow curves is found at reverse shear strains of approximately one-half the forward pre-strain in all examined cases. It follows that the estimation of internal stresses, τ_b, from the permanent softening measurements is well sustained. The values of τ_b as well as the contribution of back stress to the work hardening are listed in Table 1. The difference in the values of back-stress obtained by this approach can be ascribed to the different twin structure (volume fraction or twin thickness) present in these

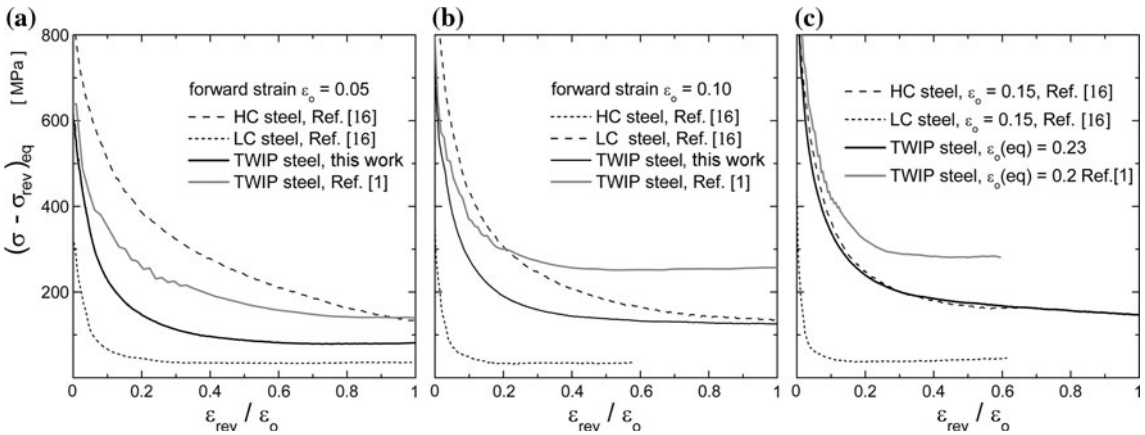

Fig. 4 Evolution of the transient softening for different levels of forward pre-strain. Data extracted from Refs. [1, 12] are included

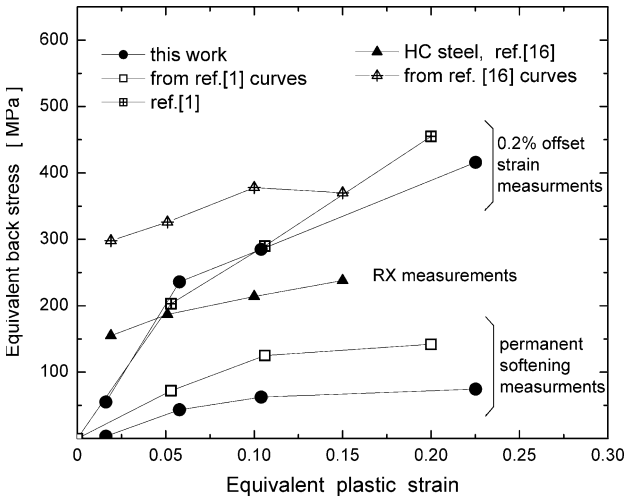

Fig. 5 Evolution of the equivalent back stress as a function of the equivalent plastic strain, for the different materials and measurement methods

Table 1 Results of permanent softening measurements on Bauschinger tests

Pre-strain, γ_o	τ (MPa)	τ_b (MPa)	$\tau_b/\tau - \tau_o^a$	σ_{eq} (MPa)	$\sigma_{b,eq}$ (MPa)
0.03	285	2 ± 2	0.03	494	0–5
0.10	355	25 ± 5	0.18	615	43
0.18	424	36 ± 5	0.18	734	62
0.40	560	43 ± 10	0.13	970	74

[a] $\tau_o = 220 \pm 10$ MPa

materials at a given strain level due to differences in the initial microstructure or texture as discussed below. Nevertheless, data show a similar evolution of the back stress with strain. Additionally, this contribution reaches a maximum value of approximately 20%. This result indicates that no outstanding BE is observed in the present TWIP steel by means of permanent softening measurements.

Discussion of the grain size and texture influence on BE effect

The theory of back stress development in materials with undeformable particles is well known. If shear loops accumulate at particles these give rise to a back stress which results in the kinematic hardening [33]. This back stress can be considered either in terms of shear loops accumulated in the particles or on a continuum basis, following the methods developed by Eshelby [34]. If the material is strained, the mean stress acting uniformly in the matrix is [22]:

$$\tau_b = 2\gamma_a DGf\varepsilon_p^* \tag{6}$$

where γ_a is the Eshelby accommodation factor, D is the modulus correction term, f is the volume fraction of particles and ε_p^* is the unrelaxed symmetrical shear strain which can be related [22] to the number of Orowan loops around the particles, n, by:

$$\varepsilon_p^* = \frac{nb}{4r} \tag{7}$$

where r is the radius of the particles. If no plastic relaxation occurs by particle deformation or secondary slip, nor diffusion nor cracking of the obstacles, the strain ε_p^* is equal to the applied strain on the slip system. Otherwise, only the number of stable loops should be taken into account. Therefore, the most important factor is the volume fraction of "undeformable obstacles". Additionally, it is important to evaluate the relaxation which should depend on the obstacle characteristics, in the present case on twin thickness. For TWIP steels, an adaptation of this theory can be performed. The mean random intercept length, L, of untwined matrix is given by [8]:

$$L = 2t\left(\frac{1-f_t}{f_t}\right) \tag{8}$$

where t is the twin thickness and f_t the twin volume fraction. For low twin volume fractions, it is possible to use $L \approx 2t/f_t$. Additionally, if the particle radius on Eq. 7 is changed by the twin thickness, from Eqs. 6–8 the following relation is obtained:

$$\tau_b = \frac{CGbn}{L} \tag{9}$$

where C is a constant. This relation was used by Bouaziz et al. [1] in their work hardening modeling of TWIP steel. We prefer to discuss the present results in terms of the volume fraction and the relaxation mechanism instead of twinning spacing and number of loops.

Regarding the grain size effect on back stress, grain size also has a significant influence on twinning stress and hence, on twin volume fraction. It has been recently published that, in Fe–22Mn–0.6C TWIP steels, the twinning stress dependence on grain size follows a Hall–Petch-type relation [6]. According to this work, in the present TWIP steel with an average grain size of 50 μm the influence of grain size on twinning stress is negligible whereas in Bouaziz's material this influence is significant. As the twinning stress in Bouaziz's material is much higher than in the present material a smaller twin volume fraction is expected in their material, and successively a lower back stress. Bouaziz et al. estimate $f_t \sim 0.05$ (at 0.2 true strain, Eq. 1 of Ref [1]) while for the present material with $D = 50$ μm we estimate $f_t \sim 0.1$. According to relation 6, these volume fractions lead to a higher back-stress for the

present material than that of Bouaziz's, which is contrary to the experimental results. This indicates that the twin volume fraction alone cannot explain the observed differences in the back-stress. In the present Fe–22Mn–0.6C TWIP steel a significant influence of grain size on twin thickness has been observed. At the same strain level (below 0.1 true strain), twin thickness ranged between 30 and 60 nm has been estimated in large grain size materials (average grain size of 15–20 μm) [35, 36] whereas in a fine grain size material (average grain size of 3 μm) thinner twins with thickness ranged between 10 and 40 nm have been observed [37]. These observations suggest that thicker twins are expected in the present TWIP steel than in that of Bouaziz's. Furthermore, thicker twins exhibit smaller twin plastic resistance according to Gil Sevillano [8] and therefore, less number of dislocation pile-ups can be maintained at twin boundaries without plastic relaxation which is consistent with the experimental results shown in Fig. 5.

On the other hand, as the stress required to create twins in a microstructure (twinning stress) is strongly influenced by the grain orientation [6] the twin volume fraction is dependent on grain orientation as well. In the present TWIP steel, the initial texture is very weak as shown in the inverse pole figures of Fig. 1b. Therefore, a noticeable in-plane plastic anisotropy for rolled sheets is not expected. However, no information on texture was provided by Bouaziz et al. Therefore, we cannot rule out that differences between the texture of Bouaziz's material and the present steel are the cause of differences in permanent softening.

It can be concluded that the difference in the permanent softening measured in both materials can be mainly ascribed to twin thickness and texture effects. However, the role of partial dissolution of dislocation cell structures [38] and/or untwining phenomena [39] under reversal straining, on the reduction of the isotropic/kinematical stress contributions and the permanent softening effect, cannot be neglected at the present state of knowledge.

Transient softening, comparison of BE data of TWIP steels and spheroidized steels

As explained above, the determination of back stresses from the BE is very sensitive to the reverse strain at which back stress is measured. Therefore, in addition to the previous analysis based on permanent softening determinations, it is useful to analyze the transient softening of the present TWIP steel in comparison to reported BE data [1, 16]. Figure 4 shows the evolution of the softening along the transient during reverse strain for different pre-strains in both TWIP steels and two spheroidized steels, a high-carbon (HC) steel and a low carbon (LC) steel having a volume fraction of cementite of $f_p = 0.17$ and $f_p = 0.005$, respectively. The comparison with spheroidized steels is interesting because in these materials Wilson and Bate [17] performed X-ray analysis of back stresses, obtaining values of around 200 MPa and 10–40 MPa on HC and LC steel, respectively, Fig. 5. An attempt to determine values of the back stress using the 0.2% offset strain approach from the curves of Wilson and Bate [17] for the HC steel was made. Those values, given in Fig. 5, are up to 2 times higher than RX determinations. This clearly shows that back stress determination by the 0.2% offset strain approach can lead to a significant overestimation of back-stresses.

As it can be seen in Fig. 4, while data of spheroidized steels show a behavior quite independent on the amount of preceding forward strain, data of TWIP steels shows an increasing amount of both transient and permanent softening effects with increasing pre-strain, due to the dynamic evolution of the twin volume fraction. Figure 4a shows that both TWIP steels have an intermediate transient softening in comparison with the spheroidized steels at a forward equivalent pre-strain of $\varepsilon_o = 0.05$. At a pre-strain of $\varepsilon_o = 0.10$, the transient softening in TWIP steels is also lower than that of the HC steel during the first part of the reverse strain. At a larger pre-strain, $\varepsilon_o = 0.2$, the curve of the TWIP steel from Ref. [1] shows larger transient softening than that of the HC steel, while the present data of the TWIP steel shows practically the same behavior than that of the HC steel. Taking into account the X-ray measurements by Wilson and Bate, it can be deduced that 200–250 MPa should be an upper limit for the back stresses in the present TWIP steel, representing approximately 20% to the total flow stress and 40% of the total work hardening. In the case of Bouaziz's steel, 250 MPa should be an upper limit except at $\varepsilon_o = 0.20$, where the transient softening is larger than that of the HC steel, Fig. 4c.

Conclusions

Summarizing, we show new experimental data on the Bauschinger effect in a Fe–22Mn wt%–0.6C wt% TWIP steel. The mechanical behavior upon load reversal shows transient and permanent softening effects. Determination of the internal stress from the magnitude of the permanent softening yields a contribution to work hardening of the order of 20%. Comparison of the transient softening with reported data on spheroidized steels shows that the back stress contribution should be lower than the 40% of the total work hardening. Finally, we want to point out that further efforts should be devoted to check the level of internal stresses by diffraction experiments, and study the substructure evolution under reversal strain to sustain the

present rationalization of the BE in terms of back stresses. The role of partial dissolution of dislocation cell structures [38], and/or untwining phenomena [39] on the reduction of the isotropic and kinematical stress contribution under reversal straining could not be neglected at the present state of knowledge.

Acknowledgements The authors would like to acknowledge the financial support by the German Research Foundation within the framework of the SFB 761 "steel ab initio" and the CICYT grant MAT2009-14452 awarded by the Spanish Ministry of Science and Innovation.

References

1. Bouaziz O, Allain S, Scott C (2008) Scripta Mater 58:484
2. Grässel O, Krüger L, Frommeyer G, Meyer LW (2000) Int J Plast 16:1391
3. Frommeyer G, Brüx U, Neumann P (2003) ISIJ Int 43:438
4. Ueji R, Tsuchida N, Terada D, Tsuji N, Tanaka Y, Takemura A, Kunishige K (2008) Scripta Mater 59:963
5. Gutierrez-Urrutia I, Zaefferer S, Raabe D (2009) Scripta Mater 61:737
6. Gutierrez-Urrutia I, Zaefferer S, Raabe D (2010) Mater Sci Eng A 527:3552
7. Lu L, Shen Y, Chen X, Quian L, Lu K (2004) Science 304:422
8. Gil Sevillano J (2009) Scripta Mater 60:336
9. Prager W (1955) Prog Inst Mech Eng 169:41
10. Figueiredo RB, Corrêa ECS, Monteiro WA, Aguilar MTP, Cetlin PR (2010) J Mater Sci 45:804. doi:10.1007/s10853-009-4003-9
11. Zhang WH, Wu JL, Wen YH, Ye JJ, Li N (2010) J Mater Sci 45:3433. doi:10.1007/s10853-010-4369-8
12. Das D, Chattopadhyay PP (2009) J Mater Sci 44:2957. doi:10.1007/s10853-009-3392-0
13. Uslu MC, Canadinc D (2010) J Mater Sci 45:1683. doi:10.1007/s10853-009-4157-5
14. Martin JW (1980) Micromechanisms in particle-hardened alloys. Cambridge University Press, Cambridge
15. Brown LM (1977) Scripta Metall 11:127
16. Wilson DV, Bate PS (1986) Acta Metall 34:1107
17. Senk D, Emmerich H, Rezende J, Siquieri R (2007) Adv Eng Mater 9:695
18. G'Sell C, Boni S, Shrivastava S (1983) J Mater Sci 18:903. doi:10.1007/BF00745590
19. Bouvier S, Haddadi H, Levée P, Teodosiu C (2006) J Mater Proc Technol 172:96
20. Lopes W, Corrêa ECS, Campos HB, Aguilar MTP, Cetlin PR (2009) J Mater Sci 44:441. doi:10.1007/s10853-008-3121-0
21. Wilson DV (1965) Acta Metall 13:807
22. Atkinson JD, Brown LM, Stobbs WM (1974) Philos Mag 30:1247
23. Moan GD, Embury JD (1979) Acta Metall 27:903
24. Lloyd DJ (1977) Acta Metall 25:459
25. del Valle JA, Romero R, Picasso AC (2001) Mater Sci Eng A 311:100
26. Stolz RE, Pelloux RM (1976) Metall Trans A 7:1295
27. Pragnell PB, Stobbs WM, Withers PJ (1992) Mater Sci Eng A 159:51
28. Barlat F, Ferreira Duarte JM, Gracio JJ, Lopes AB, Rauch EF (2003) Int J Plast 19:1215
29. Gracio JJ, Barlat F, Rauch EF, Jones PT, Neto VF, Lopes AB (2004) Int J Plast 20:427
30. Rauch EF, Gracio JJ, Barlat F, Lopes AB, Ferreira Duarte J (2002) Scripta Mater 46:881
31. Chang YW, Asaro RJ (1978) Met Sci 12:277
32. Karaman I, Sehitoglu H, Chumlyakov YI, Maier HJ, Kireeva IV (2001) Metall Mater Trans A 32:695
33. Embury JD (1985) Metall Trans A 16:2191
34. Eshelby JD (1957) Proc R Soc A241:376
35. Allain S (2004) PhD Thesis, Laboratoire de Physique des Matériaux, Ecole des Mines, Nancy
36. Allain S, Chateau JP, Dahmoun D, Bouaziz O (2004) Mater Sci Eng A 387–389:272
37. Barbier D, Gey N, Allain S, Bozzolo N, Humbert M (2009) Mater Sci Eng A 500:196
38. Hasegawa T, Yakou T, Karashima S (1975) Mater Sci Eng 20:267
39. Luo XY, Li M, Boger RK, Agnew SR, Wagoner RH (2007) Int J Plast 23:44